#### 1 Asymmetric response of European Northern Hemisphere near-surface wind speed to CO<sub>2</sub> removal 2 3 Zhi-Bo Li<sup>1</sup>, Chao Liu<sup>2</sup>, Cesar Azorin-Molina<sup>3</sup>, Soon-Il An<sup>2,4</sup>An<sup>4</sup>, Yang Zhao<sup>5,6</sup>, Yang Xu<sup>7</sup>, 4 Jongsoo Shin<sup>8</sup>, Deliang Chen<sup>9</sup>, Cheng Shen<sup>1,\*</sup> 5 6 <sup>1</sup> Regional Climate Group, Department of Earth Sciences, University of Gothenburg, 7 8 Gothenburg, Sweden 9 <sup>2</sup>Irreversible Climate Change Research Center, Yonsei<sup>2</sup> School of Earth and Environmental Sciences, Seoul National University, Seoul, South Korea 10 <sup>3</sup> Centro de Investigaciones sobre Desertificación, Consejo Superior de Investigaciones 11 Científicas (CIDE, CSIC-UV-Generalitat Valenciana), Climate, Atmosphere and Ocean 12 13 Laboratory (Climatoc-Lab), Moncada, Valencia, Spain 14 <sup>4</sup> Department of Atmospheric Sciences, Yonsei University, Seoul, South Korea <sup>5</sup> Frontiers Science Center for Deep Ocean Multispheres and Earth System-15 Key Laboratory of Physical Oceanography-Institute for Advanced Ocean Studies-16 Academy of the Future Ocean, Ocean University of China, Qingdao, China 17 <sup>6</sup> College of Oceanic and Atmospheric Sciences, Ocean University of China, Qingdao, China 18 19 <sup>7</sup> Department of Atmospheric Science, Yunnan University, Kunming, China 20 <sup>8</sup> Woods Hole Oceanographic Institution, Woods Hole, MA, USA <sup>9</sup> Department of Earth System Sciences, Tsinghua University, Beijing, China 21 22 23 \*Corresponding author: Cheng Shen (<a href="mailto:cheng.shen@gu.se">cheng.shen@gu.se</a>) 24 25 **Key words:** 26 27 CO2 removal; AMOC; near-surface wind; European wind; Asymmetric response; Northern hemisphere 28 29

Formatted: Not Superscript/ Subscript

### Abstract

30

31

32

33

34

35

36

37

38

39

40

41

42

43

44

45

46

47

48

Understanding the changes in near-surface wind speed (NSWS) is crucial for weather extremes prediction and wind energy management. This study examines the response of NSWS to atmospheric carbon dioxide (CO<sub>2</sub>) removal using large ensemble simulations and the of the Community Earth System Model version 1.2 (CESM1.2) and the models participating in the Carbon Dioxide Removal Model Intercomparison Project-models. Our results indicatereveal that increasing CO<sub>2</sub> levels—concentrations lead to an overall reduction weakening in the Northern Hemisphere (NH) extratropical NSWS over land. Subsequent CO2 reduction during the During the initial stage of CO2 removal (early rampdown period), NH NSWS rapidly restores NH NSWS recovers. However, this recovery stalls and enterstransitions into a declining trend during the late ramp-down period, mainly due to oppositedriven by pronounced negative NSWS trends in Europe. Notably, the We find that a concurrent rapid recovery of simultaneousthe Atlantic Meridional Overturning Circulation (AMOC) counteracts the global cooling-induced recovery of the North Atlantic air meridional air temperature gradient and theassociated westerly jet by global cooling, therefore, thus prolonging NSWS weakening in NH mid-latitudes NSWS weakening. Our findings underscore the pivotal and phase-dependent role of AMOC in modulating regulating NH extratropical NSWS variability under varying CO2 concentrations and provides, offering valuable insights for future climate adaptation strategies.

49

50

51

# 1 Introduction

The phenomena of terrestrial near-surface wind speed (~10 m above the ground; NSWS)

| 52 | "stilling" and subsequent "reversal" have been recognized for over a decade, yet significant  |    |                                    |
|----|---|----|------------------------------------|
| 53 | gaps remain in understanding these processes their underlying mechanisms (Wu et al., 2018;  |    |                                    |
|    |   |    |                                    |
| 54 | Zeng et al., 2019). Future Accurate future projections of NSWS have garnered significant  |    |                                    |
| 55 | attention partlyprimarily due to their implications for wind energy development (Karnauskas   |    | Formatted: English (United States) |
| 56 | et al., 2018; Zeng et al., 2019; Zhang and Li, 2020; Pryor et al., 2021; Shen et al., 2024).  |    |                                    |
| 57 | $Several\ studies\ \underline{based\ on\ climate\ model\ simulations}\ have\ investigated\ \underline{the\underline{future}}\ spatiotemporal$ |    |                                    |
| 58 | variations of NSWS in response to <u>increasing</u> atmospheric carbon dioxide (CO <sub>2</sub> ) forcing in                                  |    |                                    |
| 59 | the coming years until the end of this century based on climate models, ), revealing complex  |    |                                    |
| 60 | global and regional variations driven responses influenced by polar amplification and altered   |    | Formatted: English (United States) |
| 61 | land-sea thermal gradients (Bichet et al., 2012; Karnauskas et al., 2018; Shen et al., 2021; Zha  |    |                                    |
| 62 | et al., 2021; Deng et al., 2022). Future projections using these models, mostly from the  |    |                                    |
| 63 | Coupled Model Intercomparison Project Phases 5 and 6 (CMIP5 and CMIP6) (Taylor et al.,  |    |                                    |
| 64 | 2012; O'Neill et al., 2016), suggest aconsistently project robust reduction in NSWS   |    | Formatted: English (United States) |
| 65 | across the over mid-latitudes latitude land areas of the Northern Hemisphere (NH) land and  |    |                                    |
| 66 | <u>increases</u> in the 21st century, while an increase acrossparts of the Southern Hemisphere by the   |    |                                    |
| 67 | end of the 21st century (Karnauskas et al., 2018; Zha et al., 2021; Deng et al., 2022; Shen et  |    |                                    |
| 68 | al., 2022). However, the ideal CO2these idealized CO2 experiments in CMIP5 and CMIP6  |    | Formatted: English (United States) |
| 69 | mainly consider an increased carbon emission scenario by the end oftypically focus on   | /  | Formatted: English (United States) |
|    |   | // | Formatted: English (United States) |
| 70 | scenarios involving continuously rising CO <sub>2</sub> concentrations through the 21st century, and while                                    | // | Formatted: English (United States) |
|    |   | // | Formatted: English (United States) |
| 71 | the further potential CO2impacts of subsequent CO2 removal impact on NSWS hashave not   |    | Formatted: English (United States) |
|    |   |    | Formatted: English (United States) |
| 72 | been studied. Understanding examined. Clarifying this response is crucial in light of imperative,   |    | Formatted: English (United States) |
|    |   | /  | Formatted: English (United States) |
| 73 | given global decarbonization goalsobjectives and the extensiveanticipated widespread  |    | Formatted: English (United States) |
|    | 3   |    | Formatted: English (United States) |

74 deployment of wind powerenergy resources (Lei et al., 2023). 75 The irreversibility and asymmetry of various climate phenomena have been investigated underthrough CO2 ramp-up and ramp-down experiments using the global climate models. 76 Formatted: English (United States) Many studies used have employed the standard CMIP "1pctCO2" experiment as the ramp-up 77 periodexperiment, in which the CO<sub>2</sub> concentration gradually increases at a rate of 1% per year 78 79 for 140 years until it quadruples relative to pre-industrial levels (Eyring et al., 2016). On this 80 basis, different ramp-down scenarios of ramp-down period arehave been performed to 81 studyassess the reversibility of CO<sub>2</sub>-induced climate change (Wu et al., 2010; Cao et al., 2011; Formatted: English (United States) Boucher et al., 2012; MacDougall, 2013; Wu et al., 2014; Ma et al., 2016; Field and Mach, 82 2017; Ehlert and Zickfeld, 2018). Meanwhile To systematically explore such scenarios, the 83 Carbon Dioxide Removal Model Intercomparison Project (CDRMIP) in CMIP6 has been 84 launched to provide 1pctCO2-carbon dioxide removal experiment as the ramp-down period, 85 in which the climate initiates from the end of the 1pctCO2 experiment and the evolution of 86 CO<sub>2</sub> concentration mirrors that in the 1pctCO<sub>2</sub> experiment (Keller et al., 2018). And These 87 Formatted: English (United States) 88 experiments facilitate evaluation of climate responses and the projectionassociated Formatted: English (United States) 89 uncertainties related to differentstemming from model frameworks could also be investigated Formatted: English (United States) 90 by these experiments differences (Zhang et al., 2023; Jin et al., 2024; Su et al., 2024). 91 Following the CDRMIP protocol (Keller et al., 2018), An et al. (2021) conducted largeensemble simulations of CO2 ramp-up and ramp-down simulations using the Community 92 Earth System Model version 1.2 (CESM1.2). It is found that major ocean circulation systems, 93 particularly the Atlantic Meridional Overturning Circulation (AMOC), shows a unique 94

delayed recovery that significantly shapes the responses of other climatic factors (An et al.,

| 1   |   |  |
|-----|---|--|
| 96  | 2021; Oh et al., 2022). On this basis, followingSubsequent studies extend to expanded on these              | <br>Formatted: English (United States) |
| 97  | results to examine implications for the hydrological cycle (Yeh et al., 2021; Kim et al., 2022;             | <br>Formatted: English (United States) |
| 98  | Kug et al., 2022; Im et al., 2024), El Niño-Southern Oscillation (Liu et al., 2023a, b; Pathirana           |  |
| 99  | et al., 2023), Hadley cell (Kim et al., 2023), gross primary productivity (Yang et al., 2024) and           |  |
| 100 | mid-latitude storm tracks (Hwang et al., 2024), all showingdemonstrating varying degrees of                 | <br>Formatted: English (United States) |
| 101 | irreversibility. For the aspect of Regarding wind speed, Hwang et al. (2024) found that reported            |  |
| 102 | enhanced cyclone-related surface wind extremes become more frequent in southern North                       | <br>Formatted: English (United States) |
| 103 | America and Europe induring the late CO <sub>2</sub> removal period, while changes in. However, the         | <br>Formatted: English (United States) |
| 104 | responses of mean NSWS under these CO2 scenarios have received little attention.                            | Formatted: English (United States)     |
| 105 | -Given that CESM has a reasonable performance CESM's demonstrated capability in                             | Formatted: English (United States)     |
| 106 | reproducing global historical NSWS patterns (Shen et al., 2022), and considering the                        |  |
| 107 | importance of wind energy resources in the NH mid-latitudes are expected to be significantly                |  |
| 108 | developed in the NH mid-latitudes (Pryor et al., 2020). We are motivated to investigate how                 |  |
| 109 | NSWS in the NH mid-latitudes would respond to <u>potential</u> future CO <sub>2</sub> removal-by using the. |  |
| 110 | To ensure robustness, we analyze results from CESM1.2 simulations and alongside those from                  | Formatted: English (United States)     |
| 111 | three available CMIP6 models participating <u>in</u> the CDRMIP <del>-project</del> .                       | Formatted: English (United States)     |
| 112 |   |  |
| 113 | 2 Data and Method   |  |
| 114 | 2.1 CESM1.2 Simulations   |  |
| 115 | The CESM1.2 (Hurrell et al., 2013) includes the atmosphere (Community Atmospheric                           |  |
|     |   |  |

Model version 5), ocean (Parallel Ocean Program version 2), sea ice (Community Ice Code

version 4), and land models (Community Land Model version 4). The atmospheric

116

modelcomponent features a horizontal resolution of approximately 1° and 30 vertical levels

(Neale et al., 2012). The ocean model comprises component includes 60 vertical levels, with a

longitudinal resolution of about 1° and a latitudinal resolution of about 0.3° near the equator,

increasing gradually to about 0.5° near the poles (Smith et al., 2010). The land

modelcomponent includes the carbon-nitrogen cycle (Lawrence et al., 2011).

The experiment followed idealized CO<sub>2</sub> scenarios in two phases (An et al., 2021). In the first phase, the CO<sub>2</sub> concentration was held constant at 367 ppm, representing present-day levels, and the model is integrated for 900 years. In the second phase, the CO<sub>2</sub> concentration increased from 367 ppm to 1,478 ppm at a rate of 1% per year over 140 years (2001–2140: ramp-up period), then decreased back to 367 ppm at the same rate over the next 140 years (2141–2280: ramp-down period). After the ramp-down period, CO<sub>2</sub> levels were stabilized at 367 ppm for 220 years (2281–2500: stabilization period). This second phase was run with 28 ensemble members, each starting from different initial conditions taken from the present-day period, representing various phases of multi-decadal climate oscillations such as the Atlantic Multidecadal Oscillation and Pacific Decadal Oscillation. Such large ensemble simulations provide a sufficient tool to separate the forced responses from internal variability, making it effective in assessing forced changes in regional NSWS (Li et al., 2019; Deser et al., 2020; Zha et al., 2021).

### 2.2 CDRMIP Simulations

We <u>further</u> utilized CMIP6 models in the CDRMIP to verify the results of CESM1.2. Notably, CanESM5, MIROC-ES2L, and NorESM2-LM models are the only three available

models with variables of "sfcWind" (near-surface wind speed) and "msftmz" (stream function, for calculating AMOC), and each model contains one realization. We compared terrestrial NSWS (60°S–70°N) climatology in their present-day run (CESM1.2) and piControl experiments (CanESM5, MIROC-ES2L, and NorESM2-LM) with the ERA5 (Hersbach et al., 2020), and found that the pattern correlation coefficients are 0.85, 0.81, 0.72, and 0.89 for CESM1.2, CanESM5, MIROC-ES2L, and NorESM2-LM, respectively. Indicating their reasonable abilityFor the 20°N–70°N terrestrial NSWS, the pattern correlation coefficients are 0.71, 0.59, 0.52, and 0.83, respectively (Figure S1). The magnitudes between four models and the ERA5 are comparable, and the area weighted root mean squared difference between models and ERA5 are 1.03, 1.07, 1.37, and 0.71 m s<sup>-1</sup>, respectively. These indicate an overall reasonable ability of models in reproducing the large-scale characteristics of terrestrial NSWS.

## 2.3 AMOC Index

The AMOC index was calculated as the maximum stream function value at 26.7°N in the North Atlantic (0°N–70°N, 60°W–30°E), providing a robust measure of AMOC strength and variability across different simulation phases (An et al., 2021).

## 2.4 Statistical Methods

To facilitate consistent analysis, all data were bi-linearly interpolated to a uniform 1.5° × 1.5° grid for both latitude and longitude. All calculations related to NSWS are focused on the land regions. An 11-year running mean was used for all physical variables, unless otherwise stated. To clarify and quantify the contributions of global-mean surface air temperature and AMOC to NSWS changes, we performed a bi-regression analysis. This analysis allowed us to

assess the proportion of NSWS variance explained by each factor during different periods.

161

162

163

164

165

166

167

168

169

170

171

172

173

174

175

176

177

178

179

180

160

### 3 NSWS Responses to CO<sub>2</sub> Ramp-up and Ramp-down

In the CESM1.2 simulations, the annual global-mean surface air temperature (GMST) increases by about 5°C from 2000 to 2140 (Figure 1a). This warming trend reverses during the ramp-down period (2141-2280) as CO<sub>2</sub> concentrations decrease, but although the cooling trend is less pronounced than the priorpreceding warming. During the stabilization period (2281–2500), GMST remains approximately 1°C above the year 2000 levels for about roughly 40 years before gradually declining untiltoward 2500. Spatially, the ramp-up period shows pronounced warming over high-latitude land areas and less over the oceans, whereas oceanic warming is moderate (Figure \$\frac{\$1a\$S2a}{}). The Subpolar North Atlantic (\$NA) exhibits minimal warming, known as "warming hole" or "cold blob" (Chemke et al., 2020; Keil et al., 2020; Rahmstorf, 2024), and is likely due to reduced heat transport associated with a weakening AMOC under global warming (Zhang et al., 2019). Conversely, during the ramp-down period (2141–2280), most areas cool, including the SNA (Figure \$\frac{\text{S1b}\text{S2b}}{2}\). The asymmetric surface air temperature (SAT) trendtrends over the SNA is mostly related to are largely driven by the latedelayed recovery of the AMOC during the late ramp-down period (2221-2280), which is influenced by increased salt advection feedback due to changes in the subtropic-to-subpolar salinity gradient and ocean stratification (An et al., 2021; Oh et al., 2022). During Throughout the CO<sub>2</sub> ramp-up period (2001–2140), the NH-averaged (20°N–70°N)

annual-mean NSWS decreased, consistent with projections by CMIP6 models (Zha et al., 2021;

2280) ramp-down periods (An et al., 2021). During the early ramp-down period (2141–2220), NSWS in the NH extratropics quickly rebounds rapidly to year-2000 levels at about double the rate of the ramp-up period. The corresponding Correspondingly, SAT pattern features stronger cooling over the SNA (Figure S1eS2c), similar to the ramp-up period, indicating a strengthened meridional SAT gradient. DuringIn contrast, during the late ramp-down period (2221–2280), NH extratropical NSWS trend moderate across the NH extratropicschanges moderately (Figure 1b), accompanied by a notable warming trend over the SNA and weaker cooling trends over theat high NH latitudes of the NH compared to the early ramp-down period (2141-2220) (Figures S1eS2c-d). Throughout the stabilization period (2281-2500), NH NSWS trends in the NH continue initially continues to decline, for several decades before slowly, then gradually increasing increases towards the end of the period simulation. To investigate further examine the regional reversibility of NSWS under varying CO2 foreing conditions, Figures 2a-d show the spatial patterns of NH NSWS trends during the ramp-up, ramp-down, early ramp-down, and late ramp-down periods, respectively. During the ramp-up period (2001-2140) (Figure 2a), significant negative NSWS trends dominate the prevail across mid-latitudes of in the NH. During the ramp-down period (2141–2280), this spatial pattern reverses (Figure 2b), with a pattern correlation coefficient of -0.9 (P<0.01) between the ramp-up and ramp-down periods, highlighting a substantial impactthe

Shen et al., 2022). The ramp-down period is divided into early (2141-2220) and late (2221-

181

182

183

184

185

186

187

188

189

190

191

192

193

194

195

196

197

198

199

200

201

202

Formatted: Font: +Body (等线), 10.5 pt

pronounced effect of CO2CO2 forcing on global NSWS patterns distributions. Spatial

discrepancies between two ramp-down periods are primarily observed over the Eurasia

trends (Figure 2c); however, these positive trends turn negative in Europe and diminish in North America and Central Asia in the late ramp-down period (2221–2280) (Figure 2d).

We further examined Additionally, we validated NSWS responses inusing three CMIP6 models from CDRMIP to testify the CESM1.2 based results (Figures \$253 and \$354). It is found that the time series of NSWS over the NH extratropics are generally similar across the three models (Figure \$253), as are the spatial patterns of NSWS trends (Figure \$3). However, there are also some evident \$4). Nevertheless, noticeable inter-model differences discrepancies exist between the CDRMIP models and the CESM1.2 model. A fast recovery of NSWS is observed in the NH extratropics in the CESM1.2 during the early ramp-down period (Figure 1b), while it shows overall symmetric changes in three CDRMIP models during the throughout ramp-up and ramp-down periodperiods (Figure \$2). The discrepancies are partly related to a different \$3). These differences likely stem from differing AMOC evolution evolutions among the models, a point we elaborate further in the CESM1.2, which will be discussed in the nextfollowing section.

# 4 Effect of AMOC on Modulating the NH Extratropical NSWS

Previous studies suggested indicate that hemispheric-scale NSWS changes are strongly influenced by the large-scale meridional SAT gradient (Zha et al., 2021; Deng et al., 2022; Shen et al., 2022; Li et al., 2024), with NH mid-latitude NSWS changes being closely linked to variations in the westerly jet through the due to vertical downward momentum transport of the upper-level horizontal momentum tropospheric levels (Shen et al., 2023; Shen et al., 2025). Moreover, the strength of the AMOC critically affects these regional patterns by

Formatted: Font: +Body (等线), 10.5 pt

modulating the meridional SAT gradient and the westerly jet through its control of the SNA temperature (Zhang et al., 2019; An et al., 2021; Hwang et al., 2024). Figure 3a shows the evolution of the AMOC index in the The CESM1.2, revealing simulations reveal a clear weakening trend in AMOC (~0.5 Sy decade-1) during the ramp-up period extending until about <u>year</u> 2200, followed by a rapid strengthening trendrecovery (~1.2 Sv decade<sup>-1</sup>) persisting until around year 2300. Temporal changes of AMOC are similar among (Figure 3a). By comparison, the three CDRMIP models (Figure S4), withexhibit symmetric decreasing declining and increasing recovering trends in AMOC strength during ramp-up and ramp-down periods-, respectively (Figure S5). The different responses of AMOC would influenceacross models significantly affect regional temperatureSAT gradient, further modulatethereby altering regional atmospheric circulation (Hwang et al., 2024). To disentangleelucidate the combined effects of CO2 levels and AMOC variability on NSWS variations, we analyzed the temporal evolution of meridional SAT gradients and westerly jets acrossfor both the NH and North Atlantic (NA) (Figures 3b-e). The NH meridional SAT gradient was defined as the SAT difference between midtropical (0°N-30°N) and high-latitude (60°N-\_90°N) and tropical (0°N-30°N) bands. Mid-latitude westerly jets were defined as the average 500 hPa zonal winds for 30°N-60°N. A significant negative correlation (-0.78, P<0.01) exists between the NH extratropical NSWS (Figure 1b) and the NH SAT gradient (Figure 3b), whereas a strong positive correlation (0.91, P<0.01) is detected with the NH westerly jet (Figure 3c). During the ramp-up period (2001–2140), reductions in the weakened NH SAT gradient contributed contribute to a reduced weaker westerly jet and a weakening reduced NSWS trend across extratropics. The NH extratropical NSWS trend

225

226

227

228

229

230

231

232

233

234

235

236

237

238

239

240

241

242

243

244

245

reverses Conversely, in the early ramp-down period (2141–2220) as), NSWS quickly rebounds alongside recovery of the NH-SAT gradient and westerly jet recovers. However, induring the late ramp-down period (2221-2280), the NH SAT gradient enhanced a bitstabilizes (Figure 3b), whileresulting in slow changes in both the NH westerly jet (Figure 3c) and extratropical NSWS (Figure 1b) change slow, disregarding), despite the CO2-removal-induced global cooling. These observations suggestdynamics underscore an effect from the AMOC, which strongly modulates the SAT gradient in the NA, and thus local NSWS trends. During the ramp-up period (2001–2140), the NA SAT gradient (60°W-30°E, 0°N-30°N minus 60°W-30°E, 60°N-90°N) weaken by approximately 1°C (Figure 3d), a smaller changerelatively small magnitude compared to the 6.5°C reduction in the NH SAT gradient (Figure 3b). Actually, the The NA SAT gradient changes are modulated by two combined effects: CO2-induced global warming/cooling and the AMOC strength (Zhang et al., 2019). This milder NA SAT gradient change is related to a weakened AMOC's role in transporting warm water to the SNA, which partially offsets the hemisphere-scale SAT gradient weakening induced by global warming (Figure 3d). And the weakened NA SAT gradient favors a weakened NA NSWS (Fig. 1b). In the early ramp-down period (2141–2220), the synergistic effects of global cooling and a further weakened AMOC promote a stronger enhancement of the NA SAT gradient (Figure 3d) and westerly jet (Figure 3e)., which induce a rapidly enhancement of NA NSWS (Fig. 1b). Conversely, during the late ramp-down period (2221-2280), the fastrapid recovery of the AMOC dramatically increases warm water flow to the SNA (Figure S1d), diminishes the NA SAT gradient (Figure 3d) despite the prevailing global cooling effect from CO<sub>2</sub>-removal, and leads to a weakened NA westerly jet (Figure 3e) and

247

248

249

250

251

252

253

254

255

256

257

258

259

260

261

262

263

264

265

266

267

## NSWS (Fig. 1b).

269

270

271

272

273

274

275

276

277

278

279

280

281

282

283

284

285

286

287

288

289

290

The annual mean Spatial patterns of 500 hPa zonal wind patterns winds (Figure 4S6) reflect similar tendencies to those of NSWS in the NH, particularly across mid-latitudes where enhanced zonal winds correlate with increased NSWS (Figure 2), and vice versa. Throughout the ramp-up period (2001-2140), there is a general weakening trend of westerly jets over the mid-latitude regions of the Asian and North American continents, while regional westerlies intensify over NA and Europe (Figure 4aS6a). The early ramp-down period (2141–2220) witnesses significant strengthening trend of NH westerly jets (Figure 4eS6c), propelled by global cooling and a weakened AMOC (Figure SleS2c). During the late ramp-down period (2221-2280), recovery of the AMOC causes significant weakening of westerly jets over NA and Europe by reducing the NA SAT gradient (Zhang et al., 2019; An et al., 2021; Hwang et al., 2024) (Figures 3d-e, and S5d), which correspondingly weakens NSWS over Europe (Figure 2d). To further demonstrate the effect of the Internally generated AMOC on changes in the NA SAT gradient and westerly jet, Figure 5 displays the inter-ensemble can also support our argument about the potential roles played by CO<sub>2</sub>-forced AMOC changes. To quantify how internal AMOC variability contributes to the cross-member spread of key NA climate variables, Figure 4 shows the yearly Pearson correlation coefficients betweenamong the 28 CESM ensemble members forbetween AMOC strength and (i) the AMOC, NA meridional SAT gradient, (ii) the NA westerly-jet intensity, and (iii) the European (30°-60°N-60°N, 5°W-60 °E) NSWS. The cross member Because all members share identical external forcing, these inter-ensemble correlations are not significant during the isolate internal variability.

Significant correlations thus indicate that internal AMOC fluctuations are major drivers of atmospheric variability among ensemble members. During the ramp-up period (2001-2140) but become prominent in the ), the ensemble spread of AMOC remains small, and correlations with the three metrics are weak and statistically insignificant. However, during the late rampdown period (2221-2280), underscoring the erucial effectspread of AMOC recovery on weakening substantially increases, and the correlations become statistically significant. These year-by-year correlations clearly demonstrate that larger (smaller) AMOC anomalies are associated with a weaker (stronger) NA SAT gradient-and, a reduced (enhanced) westerly jet, leading to strong reductions in and lower (higher) European NSWS. These findings indicate that the fast recovery of the AMOC plays a dominant role in shaping the westerly jet during the late ramp-down period, and consequently, the extratropical NSWS. Moreover, we performed conducted a bi-regression analysis using GMST and AMOC to fit the changes of NSWS in as explanatory variables for NH extratropies during extratropical NSWS variability across three distinct periods. During the ramp-up period (2001-2140), GMST and AMOC explain the variance of NH extratropical NSWS for 98% and 1.2%, respectively. During the early ramp-down period (2141-2220), GMST and AMOC explain 95.3% and 4.2% of the variance, respectively. While However, during the late ramp-down period (2221-2280), GMST and the relative influence of AMOC explain 24.5% and sharply increases, accounting for 73.2% of the variance, respectively. The regression results show changes in surpassing GMST (24.5%). Thus, while GMST make the dominant role in regulatingpredominantly governs NH extratropical NSWS changes during the ramp up and early ramp-down periods, when of weaker AMOC shows gradually weakening trend. But the

291

292

293

294

295

296

297

298

299

300

301

302

303

304

305

306

307

308

309

310

311

effect of variability, AMOC plays a key role emerges as the dominant factor only when its anomalies become significantly large, such as during its rapid recovery in the late ramp-down period due to the fast recovery of AMOC. The results are consistent with those in Fig. S6c, suggesting phase. Besides, we also performed similar analysis for the three CDRMIP models. Among three models and two periods, the contributions of GMST always dominate (contributions >90%) the NH extratropical NSWS changes, further supporting that the trends of the NSWS are not simply in phase with the evolution of either CO2 or thea substantial AMOC anomaly is required for AMOC to notably influence NSWS changes, as observed in CESM.

### 5 Summary and Outlook

In this study, we utilizeutilized a CESM1.2 CO2CO2 removal experiment to assessevaluate the response of NH extratropical NSWS to anthropogenic CO2 CO2 emission levels. and subsequent removal. Our analyses reveal an asymmetric response of the NH extratropical NSWS during the CO2-ramp-up (2001–2140) and ramp-down (2141–2280) periods-, driven by phase-dependent interactions between GMST changes and AMOC-related heat transport anomalies. Figure 65 summarizes the underlying physical mechanisms about how CO2 and AMOC heat transport modulate European NSWS changes.: During the ramp-up period; (Figure 5a), the gradually weakening AMOC transports less warm water northward, thereby enhancing the meridional SAT gradient and thus strengthen NH and NA NSWS. However, the counteracting effect of CO2-driven global warming strongly reduces the NH meridional SAT gradient, ultimately dominating the response and resulting in decreased NSWS shows

decreasing trends in theacross NH extratropics. During the early ramp-down period, NSWS (Figure 5b), CO2 removal-induced global cooling combines with further AMOC weakening to substantially intensifies, facilitated by the combined effects of a weakened AMOC and the global cooling induced by CO2 removal. These conditions strengthened the meridional SAT gradient and enhance the tropospheric SAT gradient, intensifying the westerly jet, enhancing NSWS at these latitudes. In contrast and increasing NH NSWS, with GMST remaining the dominant driver due to its stronger anomalies. Conversely, during the late ramp-down period, (Figure 5c), a rapid AMOC recovery of substantially increases northward heat transport, significantly weakening the AMOC leads to significant reductions in the North Atlantic NA SAT gradient and subsequently diminishing the westerly jet and NSWS. This effect is stronger than the global cooling-AMOC-driven weakening outweighs concurrent weaker GMST cooling-induced by CO2-removal, markedlystrengthening of the SAT gradient, inducing a weakening NH and NA NSWS-over Europe and resulting in an NSWS decrease over the NH.. The European NSWS changes followexhibits distinct anticlockwise trajectories in relation to CO<sub>2</sub> concentrations (Figure 7a), indicating 6a), signifying stronger NSWS during the CO<sub>2</sub> removal period than during the CO2 increasing ramp-up period at identical CO2 concentrations levels (Kim et al., 2022). Although there are also asymmetries of NSWS over Aisa and North America (Figures 7b6b-c), but the amplitudes their magnitudes are much substantially weaker than that overcompared to Europe. These phenomena imply the effectparticular importance of AMOC is crucial to variability for European NSWS. MoreoverFurthermore, three CDRMIP models from the CDRMIP reasonablygenerally replicate NH extratropical NSWS changes over the extratropics. The reason why CDRMIP

335

336

337

338

339

340

341

342

343

344

345

346

347

348

349

350

351

352

353

354

355

models can not reproduce trends but fail to capture the pronounced asymmetry found in CESM, likely due to their relatively symmetric AMOC evolutions, which yield almost linear NSWS responses. This highlights that the asymmetric NSWS response is due to the symmetric AMOC evolution during the ramp-down period, which means the AMOC's effects are linearly in these modelsresponses critically depend on nonlinear AMOC dynamics. We acknowledge several uncertainties inherent in our findings, including potential model-dependency arising from CESM's large ensemble experiment and limited realizations from the CDRMIP simulations. Future studies involving more extensive multi-model ensembles could further validate and enhance the robustness of our conclusions. Before this study, the impact of the AMOC on terrestrial NSWS changes had been less recognized. Our resultsfindings advance the understanding inwithin the wind research community, offering valuable insights into by highlighting a crucial role for ocean circulation in modulating long-term NSWS dynamicstrends. The enhanced NH NSWS during the early CO<sub>2</sub> removal period could significantly increase wind energy production (Pryor et al., 2020) but also heighten the risks of wind-related extremes (Hwang et al., 2024; Yu et al., 2024). Therefore Consequently, it is critical for monitoring efforts and climate policy formulations to consider these findings in their long-term climate strategies to optimize benefits and mitigate risks associated with wind energy and climate interventions.

# **Declaration of competing interests**

The authors declare no conflicts of interest. 377

## Acknowledgments

357

358

359

360

361

362

363

364

365

366

367

368

369

370

371

372

373

374

375

376

This work is supported by the Swedish Formas (2023-01648, 2020-00982) and the Swedish Research Council (VR: 2021-02163). Z. B. L. is also supported by the Swedish Formas (2020-00982). C.A-M. is also supported by the CSIC Interdisciplinary Thematic Platform (PTI) "PTI+ Clima y Servicios Climáticos" and the RED-CLIMA 2 (ref. LINCG24042). S.-I.A. is also supported by National Research Foundation of Korea grants funded by the Korean government (NRF-2018R1A5A1024958). C.S. is also supported by the Sven Lindqvists Forskningsstiftelse, Stiftelsen Längmanska kulturfonden (BA24-0484) and Adlerbertska Forskningsstiftelsen (AF2024-0069). The CESM simulation was conducted on the supercomputer supported by the National Center for Meteorological Supercomputer of Korea Meteorological Administration (KMA), the National Supercomputing Center with supercomputing resources, associated technical support (KSC-2021-CHA-0030), and the Korea Research Environment Open NETwork (KREONET). **Data Availability** All data used in this study are publicly available. The CESM1.2 outputs are available from https://data.mendeley.com/datasets/f5ry6hgxkw/2. CMIP6 outputs are available from the Earth System Grid Federation (https://esgf-data.dkrz.de/projects/esgf-dkrz/). And ERA5 reanalysis data are available from the European Centre for Medium-Range Weather Forecasts (https://cds.climate.copernicus.eu/cdsapp#!/dataset/reanalysis-era5-singlelevels?tab=overview). **Supplementary Information** The manuscript contains supplementary materials.

379

380

381

382

383

384

385

386

387

388

389

390

391

392

393

394

395

396

397

398

### References

401

425

426 427

428

429 430

- An, S.-I., J. Shin, S.-W. Yeh, S.-W. Son, J.-S. Kug, S.-K. Min, and H.-J. Kim (2021). Global cooling hiatus driven by an AMOC overshoot in a carbon dioxide removal scenario, *Earth's Future*, 9, e2021EF002165. <a href="https://doi.org/10.1029/2021EF002165">https://doi.org/10.1029/2021EF002165</a>
- Bichet, A., M. Wild, D. Folini, and C. Schar (2012). Causes for decadal variations of wind
   speed over land: Sensitivity studies with a global climate model, *Geophysical Research Letters*, 39(11). <a href="https://doi.org/10.1029/2012GL051685">https://doi.org/10.1029/2012GL051685</a>
- Boucher, O., P. R. Halloran, E. J. Burke, M. Doutriaux-Boucher, C. D. Jones, J. Lowe, M. A.
   Ringer, E. Robertson, and P. Wu (2012). Reversibility in an Earth System model in
   response to CO2 concentration changes, *Environmental Research Letters*, 7, 024013.
   <a href="https://doi.org/10.1088/1748-9326/7/2/024013">https://doi.org/10.1088/1748-9326/7/2/024013</a>
- Cao, L., G. Bala, and K. Caldeira (2011). Why is there is a short-term increase in global precipitation in response to diminished CO<sub>2</sub> forcing? *Geophysical Research Letters*, 38, L06703. https://doi.org/10.1029/2011GL046713
- 415 Chemke, R., L. Zanna, and L. M. Polvani (2020). Identifying a human signal in the North 416 Atlantic warming hole. *Nature Communications*, 11(1), 1–7. 417 <a href="https://doi.org/10.1038/s41467-020-15285-x">https://doi.org/10.1038/s41467-020-15285-x</a>
- Deng, K., W. Liu, C. Azorin-Molina, S. Yang, H. Li, G. Zhang, L. Minola, and D. Chen (2022).
   Terrestrial stilling projected to continue in the Northern Hemisphere mid-latitudes,
   *Earth's Future*, 10(7), e2021EF002448. <a href="https://doi.org/10.1029/2021EF002448">https://doi.org/10.1029/2021EF002448</a>
- Deser, C., F. Lehner, K. B. Rodgers, T. Ault, T. L. Delworth, P. N. DiNezio, A. Fiore, C.
   Frankignoul, J. C. Fyfe, and D. E. Horton (2020). Insights from Earth system model initial-condition large ensembles and future prospects, *Nature Climate Change*, 10(4), 277–286. <a href="https://doi.org/10.1038/s41558-020-0731-2">https://doi.org/10.1038/s41558-020-0731-2</a>
  - Ehlert, D, and K. Zickfeld (2018). Irreversible ocean thermal expansion under carbon dioxide removal, *Earth System Dynamics*, 9(1), 197–210. <a href="https://doi.org/10.5194/esd-9-197-2018">https://doi.org/10.5194/esd-9-197-2018</a>
  - Eyring, V., S. Bony, G. A. Meehl, C. A. Senior, B. Stevens, R. J. Stouffer, and K. E. Taylor (2016). Overview of the Coupled Model Intercomparison Project Phase 6 (CMIP6) experiment design and organization, *Geoscientific Model Development*, 9, 1937–1958. https://doi.org/10.5194/gmd-9-1937-2016
- Field, C. B., and K. J. Mach (2017). Rightsizing carbon dioxide removal, *Science*, *356*(6339), 706–707. <a href="https://doi.org/10.1126/science.aam9726">https://doi.org/10.1126/science.aam9726</a>
- Hersbach, H., B. Bell, P. Berrisford, S. Hirahara, A. Horányi, J. Muñoz-Sabater, J. Nicolas, C.
   Peubey, et al. (2020). The ERA5 global reanalysis, *Quarterly Journal of the Royal Meteorological Society*, 146(730), 1999-2049. https://doi.org/10.1002/qj.3803
- Hurrell, J. W., M. M. Holland, P. R. Gent, S. Ghan, J. E. Kay, and P. J. Kushner (2013). The
   community earth system model: A framework for collaborative research. *Bulletin of the American Meteorological Society*, *94*(9), 1339–1360. <a href="https://doi.org/10.1175/BAMS-D-12-00121.1">https://doi.org/10.1175/BAMS-D-12-00121.1</a>
- Hwang, J., S.-W. Son, C. I. Garfinkel, T. Woollings, H. Yoon, S.-I. An, S.-W. Yeh, S.-K., Min,
   J.-S. Kug, and J. Shin (2024). Asymmetric hysteresis response of mid-latitude storm

- tracks to CO<sub>2</sub> removal, *Nature Climate Change*, 14, 496–503. https://doi.org/10.1038/s41558-024-01971-x
- Im, N., D., Kim, S.-I., An, S., Paik, S.-K., Kim, J., Shin, S.-K., Min, et al. (2024). Hysteresis
   of European summer precipitation under a symmetric CO<sub>2</sub> ramp-up and ramp-down
   pathway, Environmental Research Letters, 19, 074030. https://doi.org/10.1088/1748 9326/ad52ad
- Jin, J., D. Ji, X. Dong, K. Fei, R. Guo, J. He, Y. Yu, et al. (2024). CAS-ESM2.0 dataset for the
   Carbon Dioxide Removal Model Intercomparison Project (CDRMIP), Advances in
   Atmospheric Sciences, 41, 989–1000. <a href="https://doi.org/10.1007/s00376-023-3089-3">https://doi.org/10.1007/s00376-023-3089-3</a>
- Karnauskas, K. B., J. K. Lundquist, and L. Zhang (2018). Southward shift of the global wind
   energy resource under high carbon dioxide emissions, *Nature Geoscience*, 11(1), 38–43.
   <a href="https://doi.org/10.1038/s41561-017-0029-9">https://doi.org/10.1038/s41561-017-0029-9</a>
- Keil, P., T. Mauritsen, J. Jungclaus, C. Hedemann, D. Olonscheck, and R. Ghosh (2020).
   Multiple drivers of the North Atlantic warming hole. *Nature Climate Change*, 10(7), 667–671. <a href="https://doi.org/10.1038/s41558-020-0819-8">https://doi.org/10.1038/s41558-020-0819-8</a>
- Keller, D. P., A. Lenton, V. Scott, N. E. Vaughan, N. Bauer, D. Ji, C. D. Jones, et al. (2018).
   The Carbon Dioxide Removal Model Intercomparison Project (CDRMIP): rationale and experimental protocol for CMIP6, Geoscientific Model Development, 11(3), 1133–1160.
   <a href="https://doi.org/10.5194/gmd-11-1133-2018">https://doi.org/10.5194/gmd-11-1133-2018</a>
- Kim, S.-K., J. Shin, S.-I. An, H.-J. Kim, N. Im, S. Xie, J.-S. Kug, and S.-W. Yeh (2022).
   Widespread irreversible changes in surface temperature and precipitation in response to
   CO<sub>2</sub> forcing, *Nature Climate Change*, 12, 834–840. <a href="https://doi.org/10.1038/s41558-022-01452-z">https://doi.org/10.1038/s41558-022-01452-z</a>
- Kim, S.-Y., Y.-J. Choi, S.-W. Son, K. M. Grise, P. W. Staten, S.-I. An, S.-W. Yeh, J.-S. Kug,
   S.-K. Min, and J. Shin (2023). Hemispherically asymmetric Hadley cell response to
   CO<sub>2</sub> removal, Science Advances, 9(30), eadg1801.
   https://doi.org/10.1126/sciadv.adg1801
- Kug, J.-S., J.-H. Oh, S.-I. An, S.-W. Yeh, S.-K. Min, S.-W. Son, J. Kam, Y.-G. Ham, and J.
   Shin (2022). Hysteresis of the intertropical convergence zone to CO<sub>2</sub> forcing, *Nature Climate Change*, 12, 47–53. <a href="https://doi.org/10.1038/s41558-021-01211-6">https://doi.org/10.1038/s41558-021-01211-6</a>
- Lawrence, D. M., K. W. Oleson, M. G. Flanner, P. E. Thornton, S. C. Swenson, P. J. Lawrence,
   et al. (2011). Parameterization improvement sand functional and structural advances in
   Version 4 of the community land model. *Journal of Advances in Modeling Earth Systems*,
   3(3), 1–27. <a href="https://doi.org/10.1029/2011ms000045">https://doi.org/10.1029/2011ms000045</a>
- Lei, Y., Z. Wang, D. Wang, X. Zhang, H. Che, X. Yue, C. Tian, J. Zhong, L. Guo, L. Li, H.
   Zhou, L. Liu, and Y. Xu (2023). Co-benefits of carbon neutrality in enhancing and
   stabilizing solar and wind energy, *Nature Climate Change*, 13, 693–700.
   <a href="https://doi.org/10.1038/s41558-023-01692-7">https://doi.org/10.1038/s41558-023-01692-7</a>
- Li, Z.-B., Y. Sun, T. Li, T. Hu, and Y. Ding (2019). Future changes in East Asian summer monsoon circulation and precipitation under 1.5 to 5 °C of warming, *Earth's Future*, 7(12), 1391–1406. https://doi.org/10.1029/2019EF001276
- Li, Z.-B., Y. Xu, H.-S. Yuan, Y. Chang, and C. Shen (2024). AMO footprint of the recent near-surface wind speed change over China, *Environmental Research Letters*, 19, 114031.

### 486 https://doi.org/10.1088/1748-9326/ad7ee4

500

501

502 503

504

505 506

507 508

509

513

514

515516

517

- Liu, C., S.-I. An, F. Jin, J. Shin, J.-S. Kug, W. Zhang, M. F. Stuecker, X. Yuan, A. Xue, X.
   Geng, and S.-K. Kim (2023a). Hysteresis of the El Niño–Southern Oscillation to
   CO<sub>2</sub> forcing, *Science Advances*, 9(31), eadh8442. <a href="https://doi.org/10.1126/sciadv.adh8442">https://doi.org/10.1126/sciadv.adh8442</a>
- Liu, C., S.-I. An, F. Jin, M. F. Stuecker, W. Zhang, J.-S. Kug, X. Yuan, J. Shin, A. Xue, X.
   Geng and S.-K. Kim (2023b). ENSO skewness hysteresis and associated changes in strong El Niño under a CO<sub>2</sub> removal scenario, *npj Climate and Atmospheric Science*, 6, 117. <a href="https://doi.org/10.1038/s41612-023-00448-6">https://doi.org/10.1038/s41612-023-00448-6</a>
- Ma, J., G. R. Foltz, B. J. Soden, G. Huang, J. He, and C. Dong (2016). Will surface winds
   weaken in response to global warming? *Environmental Research Letters*, 11, 124012.
   <a href="https://doi.org/10.1088/1748-9326/11/12/124012">https://doi.org/10.1088/1748-9326/11/12/124012</a>
- MacDougall. A. H., (2013). Reversing climate warming by artificial atmospheric carbon-dioxide removal: Can a Holocene-like climate be restored? *Geophysical Research Letters*,
   499 40(20), 5480–5485. <a href="https://doi.org/10.1002/2013GL057467">https://doi.org/10.1002/2013GL057467</a>
  - Neale, R. B., C.-C. Chen, A. Gettelman, P. H. Lauritzen, S. Park, D. L. Williamson, et al. (2012). Description of the NCAR community atmosphere model (CAM 5.0). NCAR Tech. Note NCAR/TN-486+ STR (pp. 1–12). National Center for Atmospheric Research.
  - Oh, J.-H., S.-I. An, J. Shin, and J.-S. Kug (2022). Centennial memory of the Arctic Ocean for future Arctic climate recovery in response to a carbon dioxide removal. *Earth's Future*, 10(8), e2022EF002804. https://doi.org/10.1029/2022EF002804
  - O'Neill, B. C., C. Tebaldi, D. P. Van Vuuren, V. Eyring, P. Friedlingstein, G. Hurtt, R. Knutti, E. Kriegler, et al. (2016). The scenario model intercomparison project (ScenarioMIP) for CMIP6, *Geoscientific Model Development*, 9(9), 3461–3482. <a href="https://doi.org/10.5194/gmd-9-3461-2016">https://doi.org/10.5194/gmd-9-3461-2016</a>
- Pathirana, G., J.-H. Oh, W. Cai, S.-I. An, S.-K. Min, S.-Y. Jo, J. Shin, and J.-S. Kug (2023).

  Increase in convective extreme El Niño events in a CO<sub>2</sub> removal scenario, *Science Advances*, 9(25), eadh2412. https://doi.org/10.1126/sciadv.adh2412
  - Pryor, S., and R. J. Barthelmie (2021). A global assessment of extreme wind speeds for wind energy applications, *Nature Energy*, 6(3), 268–276. <a href="https://doi.org/10.1038/s41560-020-00773-7">https://doi.org/10.1038/s41560-020-00773-7</a>
  - Pryor, S., R. J. Barthelmie, M. S. Bukovsky, L. R. Leung, and K. Sakaguchi (2020). Climate change impacts on wind power generation, *Nature Reviews Earth & Environment*, *I*(12), 627–643. <a href="https://doi.org/10.1038/s43017-020-0101-7">https://doi.org/10.1038/s43017-020-0101-7</a>
- Rahmstorf, S (2024). Is the Atlantic overturing circulation approaching a tipping point?

  Oceanography, 37(3), 16–29. https://doi.org/10.5670/oceanog.2024.501
- Shen, C., J. Zha, D. Zhao, J. Wu, W. Fan, M. Yang, and Z.-B. Li (2021). Estimating centennial-scale changes in global terrestrial near-surface wind speed based on CMIP6 GCMs,
   Environmental Research Letters, 16(8), 084039. <a href="https://doi.org/10.1088/1748-9326/ac1378">https://doi.org/10.1088/1748-9326/ac1378</a>
- Shen, C., J. Zha, Z.-B. Li, C. Azorin-Molina, K. Deng, L. Minola, and D. Chen (2022).
   Evaluation of global terrestrial near-surface wind speed simulated by CMIP6 models and
   their future projections, *Annals of the New York Academy of Sciences*, 1518(1), 249–263.
   <a href="https://doi.org/10.1111/nyas.14910">https://doi.org/10.1111/nyas.14910</a>

- 529 Shen, C., H. Yuan, Z.-B. Li, X. Yang, L. Minola, Y. Chang, and D. Chen (2023). March near-530 surface wind speed hiatus over China since 2011, *Geophysical Research Letters*, 50(15), 531 e2023GL104230. https://doi.org/10.1029/2023GL104230
- Shen, C., Z.-B. Li, H. Yuan, Y. Yu, Y. Lei, and D. Chen (2024). Increases of offshore wind
   potential in a warming world, *Geophysical Research Letters*, 50(15), e2024GL109494.
   <a href="https://doi.org/10.1029/2024GL109494">https://doi.org/10.1029/2024GL109494</a>
- Shen, C., Z.-B. Li, F. Liu, H. W. Chen, and D. Chen (2025). A robust reduction in near-surface
   wind speed after volcanic eruptions: Implications for wind energy generation, *The Innovation*, 6(1), 100734. <a href="https://doi.org/10.1016/j.xinn.2024.100734">https://doi.org/10.1016/j.xinn.2024.100734</a>

540

541

542

543

544

554

555

556

557

558 559

- Smith, R., P. Jones, B. Briegleb, F. Bryan, G. Danabasoglu, J. Dennis, et al. (2010). The parallel ocean program (POP) reference manual ocean component of the community climate system model (CCSM) and community earth system model (CESM). LAUR-01853 (pp. 1–140).
- Su, X., G. Huang, L. Wang, and T. Wang (2024). Global drought changes and attribution under carbon neutrality scenario, *Climate Dynamics*, *62*, 7851–7868. <a href="https://doi.org/10.1007/s00382-024-07310-2">https://doi.org/10.1007/s00382-024-07310-2</a>
- Taylor, K. E., R. J. Stouffer, and G. A. Meehl (2012). An overview of CMIP5 and the
   experiment design, *Bulletin of the American Meteorological Society*, 93(4), 485–498.
   <a href="https://doi.org/10.1175/BAMS-D-11-00094.1">https://doi.org/10.1175/BAMS-D-11-00094.1</a>
- Wu, J., J. Zha, D. Zhao, and Q. Yang (2018). Changes in terrestrial near-surface wind speed
   and their possible causes: an overview, *Climate Dynamics*, 51(5–6), 2039–2078.
   <a href="https://doi.org/10.1007/s00382-017-3997-y">https://doi.org/10.1007/s00382-017-3997-y</a>
- Wu, P., J. Ridley, A. Pardaens, R. Levine, and J. Lowe (2014). The reversibility of CO<sub>2</sub> induced
   climate change, *Climate Dynamics*, 45, 745–754. <a href="https://doi.org/10.1007/s00382-014-2302-6">https://doi.org/10.1007/s00382-014-2302-6</a>
  - Wu, P., R. Wood, J. Ridley, and J. Lowe (2010). Temporary acceleration pf the hydrological cycle in response to a CO<sub>2</sub> rampdown, *Geophysical Research Letters*, *37*(12), L043730. https://doi.org/10.1029/2010GL043730
  - Yang, Y.-M., J. Shin, S.-W. Park, J.-H. Park, S.-I. An, J.-S., Kug, S.-W. Yeh, et al. (2024). Fast reduction of Atlantic SST threatens Europe-wide gross primary productivity under positive and negative CO2 emissions. *npj Climate and Atmospheric Science*, 7(1), 117. https://doi.org/10.1038/s41612-024-00674-6
- Yeh, S.-W., S.-Y. Song, R. P. Allan, S.-I. An, and J. Shin (2021). Contrasting response of
   hydrological cycle over land and ocean to a changing CO<sub>2</sub> pathway, *npj Climate and Atmospheric Science*, 4, 53. <a href="https://doi.org/10.1038/s41612-021-00206-6">https://doi.org/10.1038/s41612-021-00206-6</a>
- Yu, Y., Z.-B. Li, Z. Yan, H. Yuan, and C. Shen (2024). Projected emergence seasons of year maximum near-surface wind speed, Geophysical Research Letters, 51(2).
   <a href="https://doi.org/10.1029/2023GL107543">https://doi.org/10.1029/2023GL107543</a>
- Zeng, Z., A. D. Ziegler, T. Searchinger, L. Yang, A. Chen, K. Ju, S. Piao, L. Z. Li, P. Ciais, and
   D. Chen (2019). A reversal in global terrestrial stilling and its implications for wind
   energy production, *Nature Climate Change*, 9(12), 979–985.
   <a href="https://doi.org/10.1038/s41558-019-0622-6">https://doi.org/10.1038/s41558-019-0622-6</a>
- 571 Zha, J., C. Shen, Z.-B. Li, J. Wu, D. Zhao, W. Fan, M. Sun, C. Azorin-Molina, and K. Deng

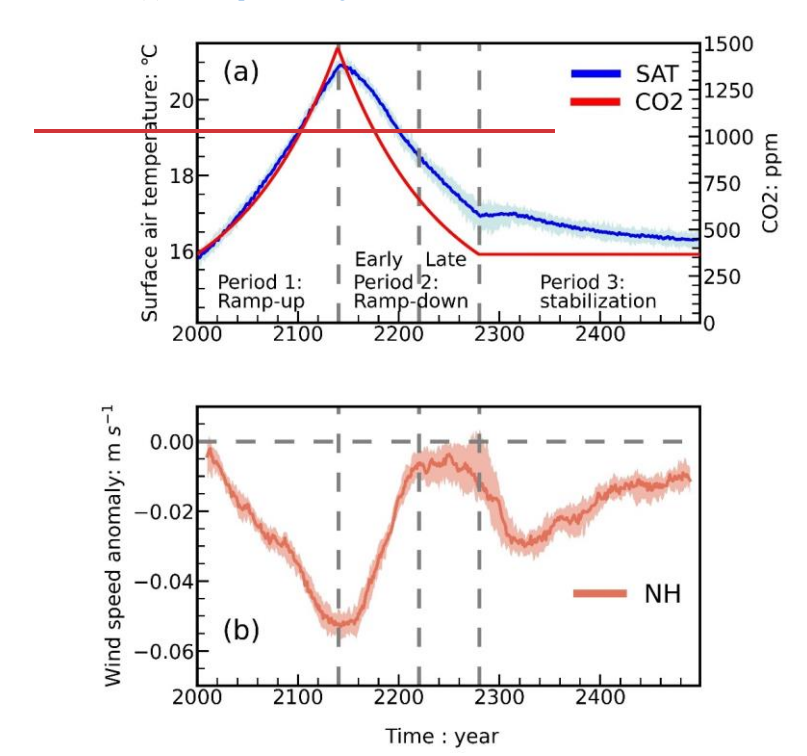
(2021). Projected changes in global terrestrial near-surface wind speed in 1.5° C–4.0° C global warming levels, *Environmental Research Letters*, *16*(11), 114016. https://doi.org/10.1088/1748-9326/ac2fdd

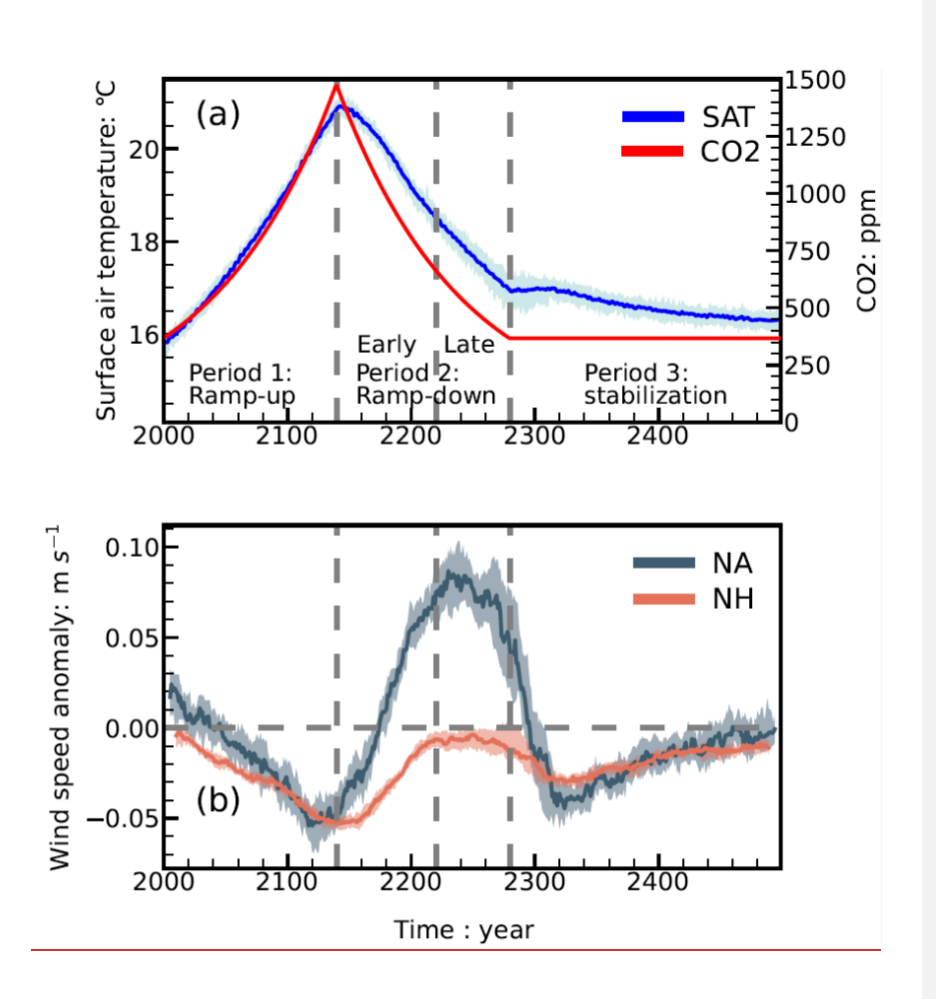
Zha, J., C. Shen, J. Wu, D. Zhao, W. Fan, H. Jiang, and T. Zhao (2023). Evaluation and projection of changes in daily maximum wind speed over China based on CMIP6. *Journal of Climate*, 36(5), 1503–1520. https://doi.org/10.1175/JCLI-D-22-0193.1

 Zhang, R., R. Sutton, G. Danabasoglu, Y. O. Kwon, R. Marsh, S. G. Yeager, D. E. Amrhein, and C. M. Little (2019). A review of the role of the Atlantic meridional overturning circulation in Atlantic multidecadal variability and associated climate impacts, *Reviews of Geophysics*, 57(2), 316–375. <a href="https://doi.org/10.1029/2019RG000644">https://doi.org/10.1029/2019RG000644</a>

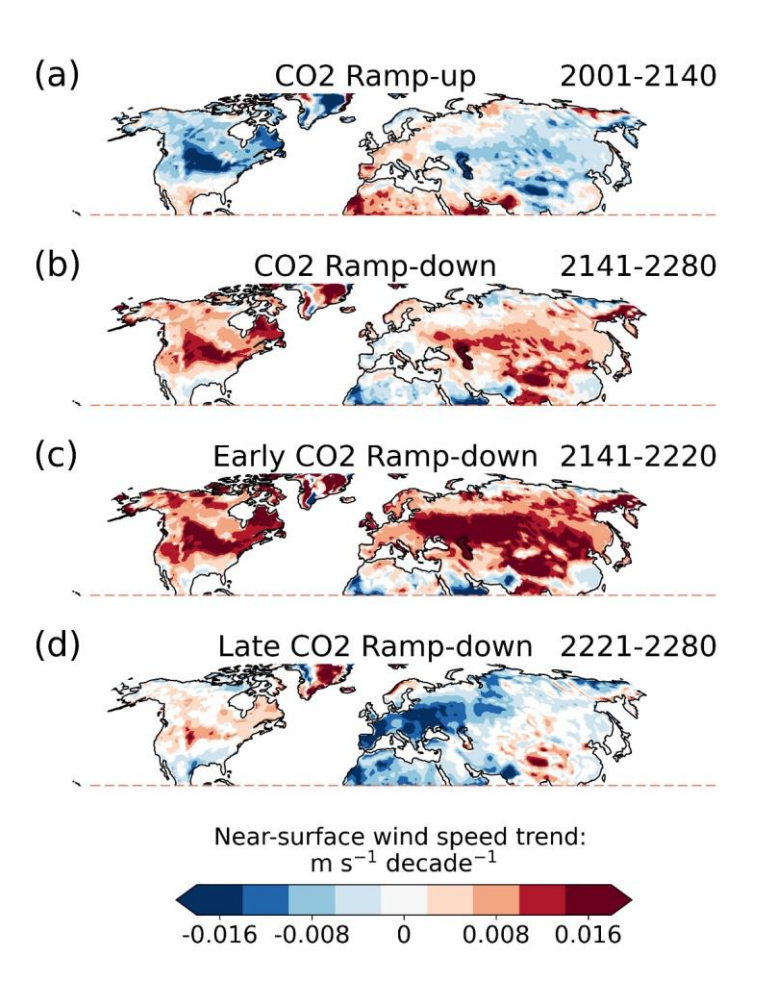
Zhang, S., and X. Li (2020). Future projections of offshore wind energy resources in China using CMIP6 simulations and a deep learning-based downscaling method, *Energy*, 217, 119321. https://doi.org/10.1016/j.energy.2020.119321

Zhang, S., X. Qu, G. Huang, and P. Hu (2023). Asymmetric response of South Asian summer monsoon rainfall in a carbon dioxide removal scenario, *npj Climate and Atmospheric Science*, 6(1), 10. <a href="https://doi.org/10.1038/s41612-023-00338-x">https://doi.org/10.1038/s41612-023-00338-x</a>

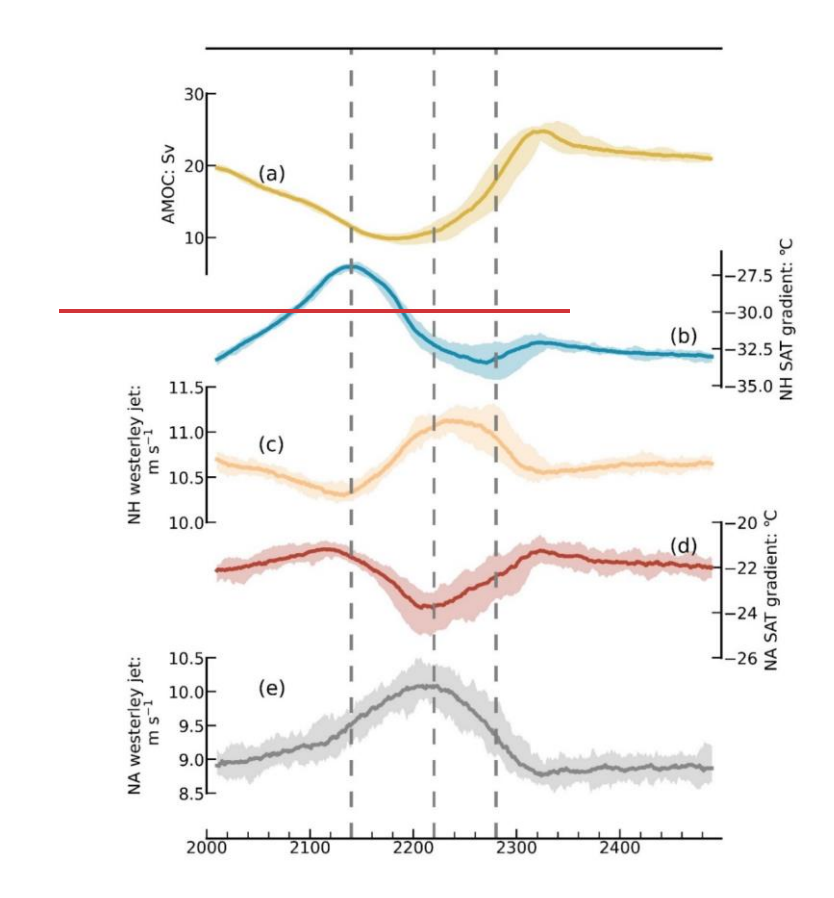


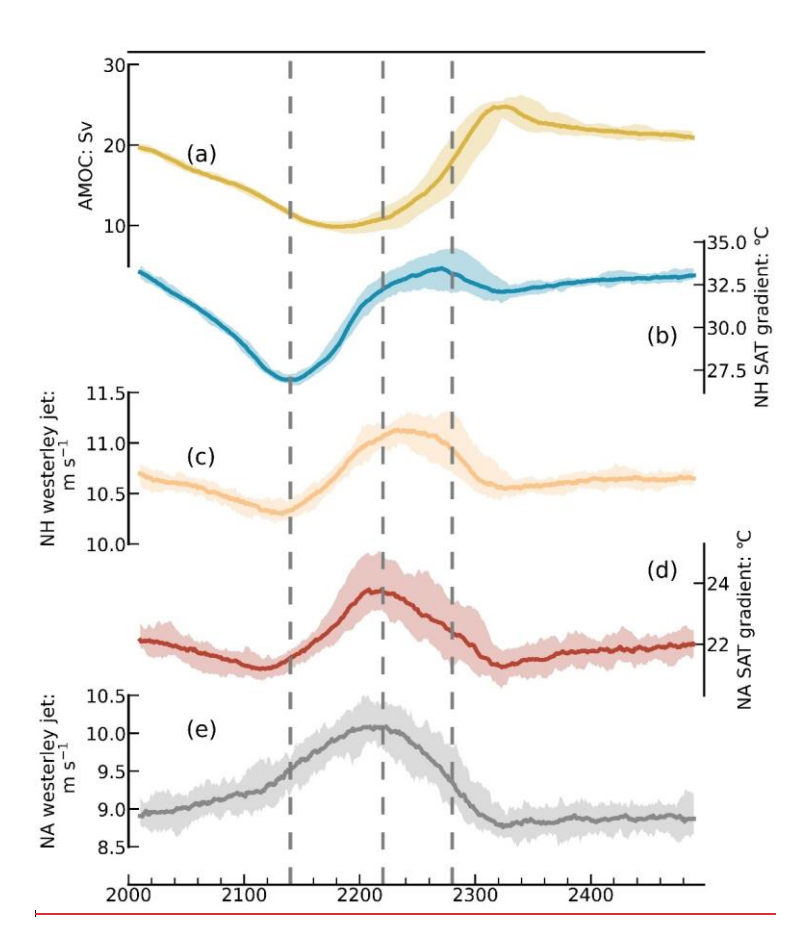


**Figure 1.** (a) Temporal changes of the annual global mean surface air temperature (SAT; unit: °C) (blue) and CO<sub>2</sub> concentration (unit: ppm) (red). The solid lines represent the ensemble means, while the shaded areas indicate the 25th to 75th percentile range across 28 members. Three dashed gray lines mark the years 2140, 2220, and 2280, highlighting important temporal milestones in the experiment. (b) Temporal changes of annual-mean terrestrial near-surface wind speed (NSWS; unit: m s<sup>-1</sup>) over Northern Hemisphere (20°N–70°N) (orange):) and North Atlantic (0°N–70°N, 60°W–30°E) (dark blue). Anomalies are calculated relative to the average NSWS of the constant CO<sub>2</sub> scenario. An 11-year running mean has been applied to smooth out inter-annual variability.

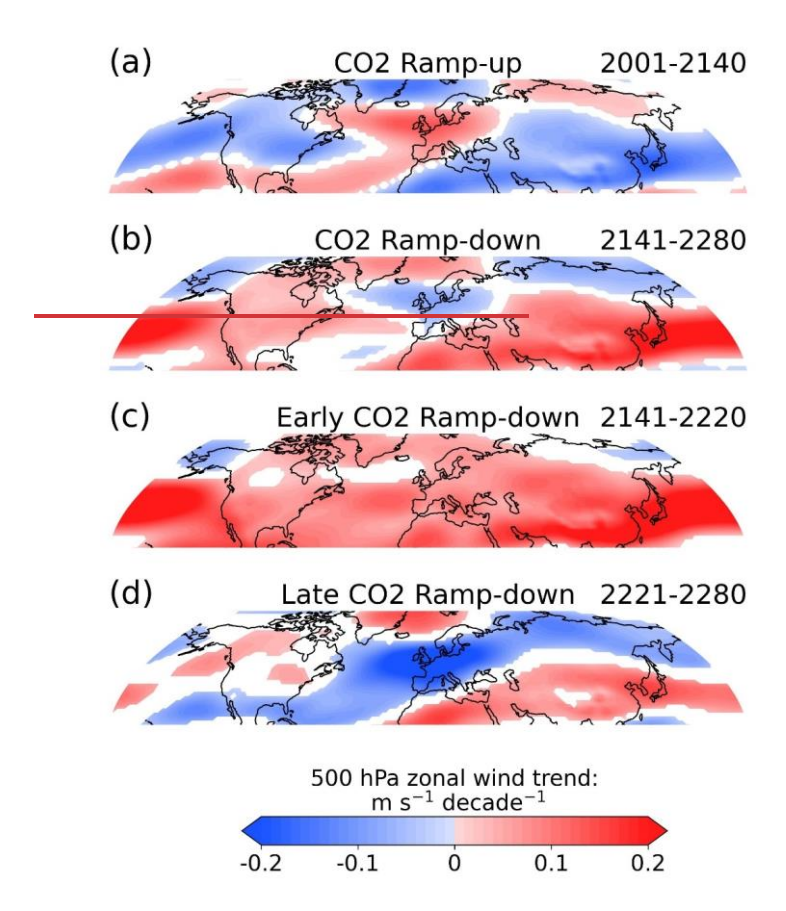


**Figure 2.** (a) Decadal trend in annual-mean near-surface wind speed (unit: m s<sup>-1</sup> decade<sup>-1</sup>) during the CO<sub>2</sub> ramp-up period (2001–2140). Grid points with shadings denote the tendencies are significant at the 0.05 level. (b–d) Same as (a), but for tendencies during the CO<sub>2</sub> ramp-down period (2141–2280), early CO<sub>2</sub> ramp-down period (2141–2220), and late CO<sub>2</sub> ramp-down period (2221–2280), respectively.

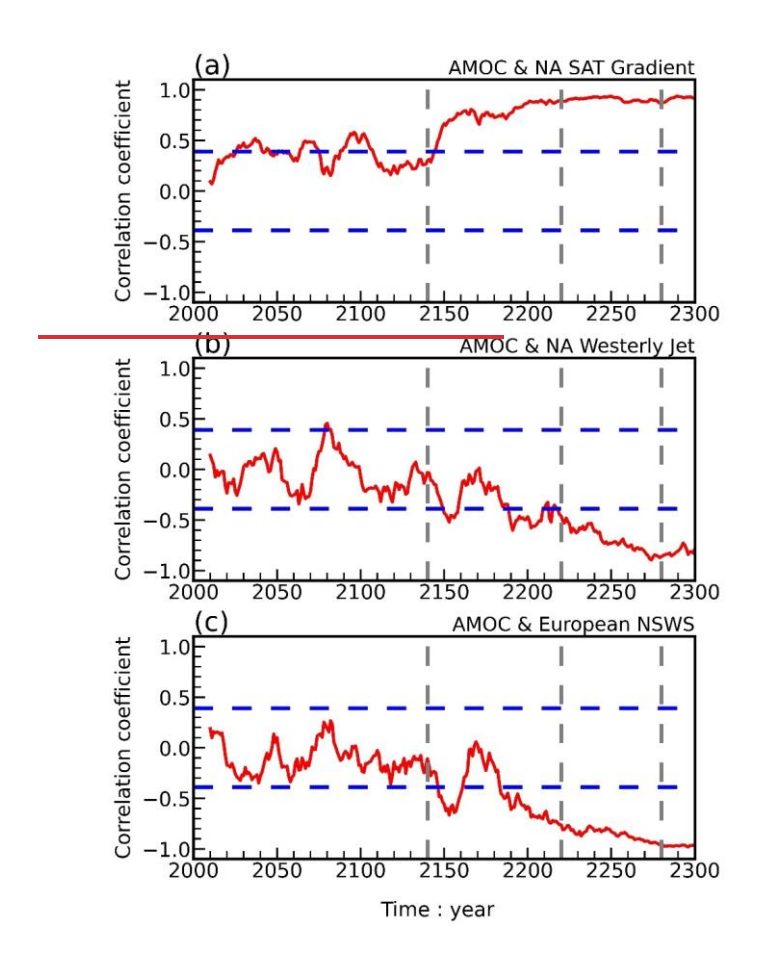




**Figure 3.** (a) Temporal changes of the Atlantic Meridional Overturning Circulation index (unit: Sv). The solid line represents the ensemble mean, and the shaded area shows the 25th to 75th percentile range of 28 ensemble members. Dashed gray lines at 2140, 2220, and 2280 denote significant temporal markers. (b–e) Same as (a), but for Northern Hemisphere (NH) surface air temperature gradient (600°N–9030°N minus 060°N–3090°N; in °C), NH westerly jet strength (the average for 30°N–60°N; in m s<sup>-1</sup>) at 500 hPa, North Atlantic (NA, 60°W–30°E) surface air temperature gradient (600°N–9030°N minus 060°N–3090°N; in °C), and NA westerly jet strength (the average for 30°N–60°N, 60°W–30°E; in m s<sup>-1</sup>) at 500 hPa, respectively. An 11-year running mean has been applied to smooth out inter-annual variability.



**Figure 4.** (a) Tendencies of ensemble mean annual mean 500 hPa zonal wind (unit: m s<sup>-1</sup> decade<sup>-1</sup>) during the CO<sub>2</sub>-ramp up period (2001–2140). Grid points with shadings denote the tendencies are significant at the 0.05 level. (b d) Same as (a), but for tendencies during the CO<sub>2</sub>-ramp down period (2141–2280), early CO<sub>2</sub>-ramp down period (2141–2220), and late CO<sub>2</sub>-ramp down period (2221–2280), respectively.



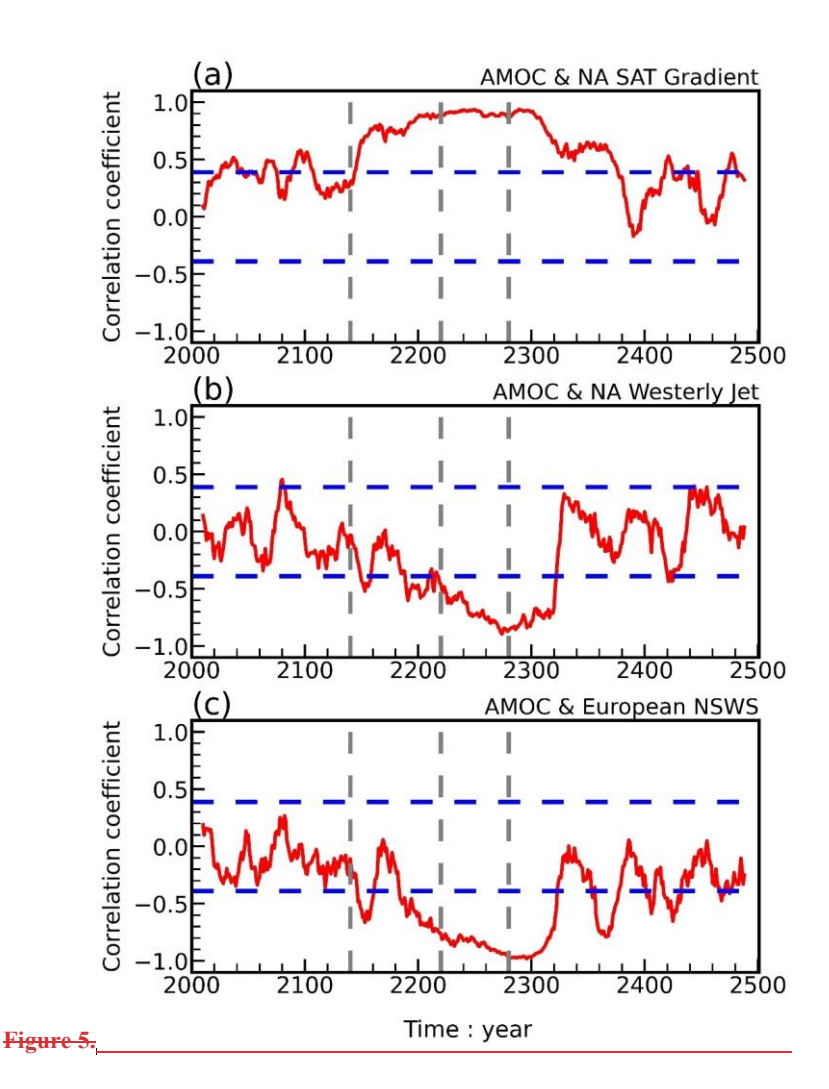
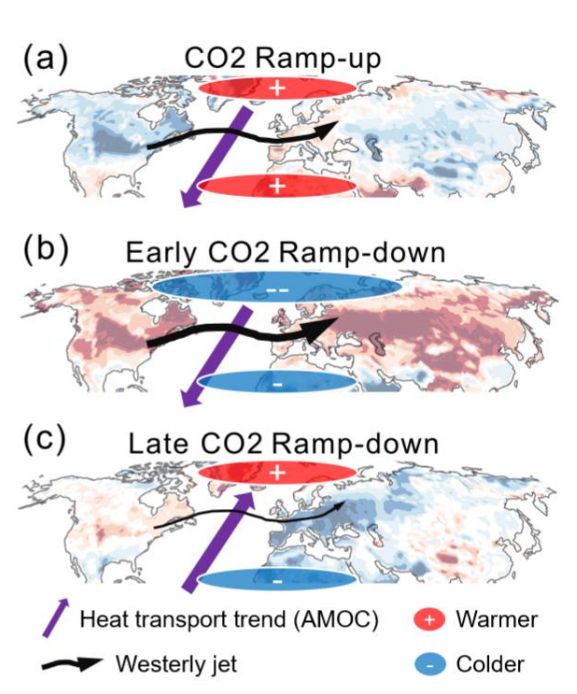
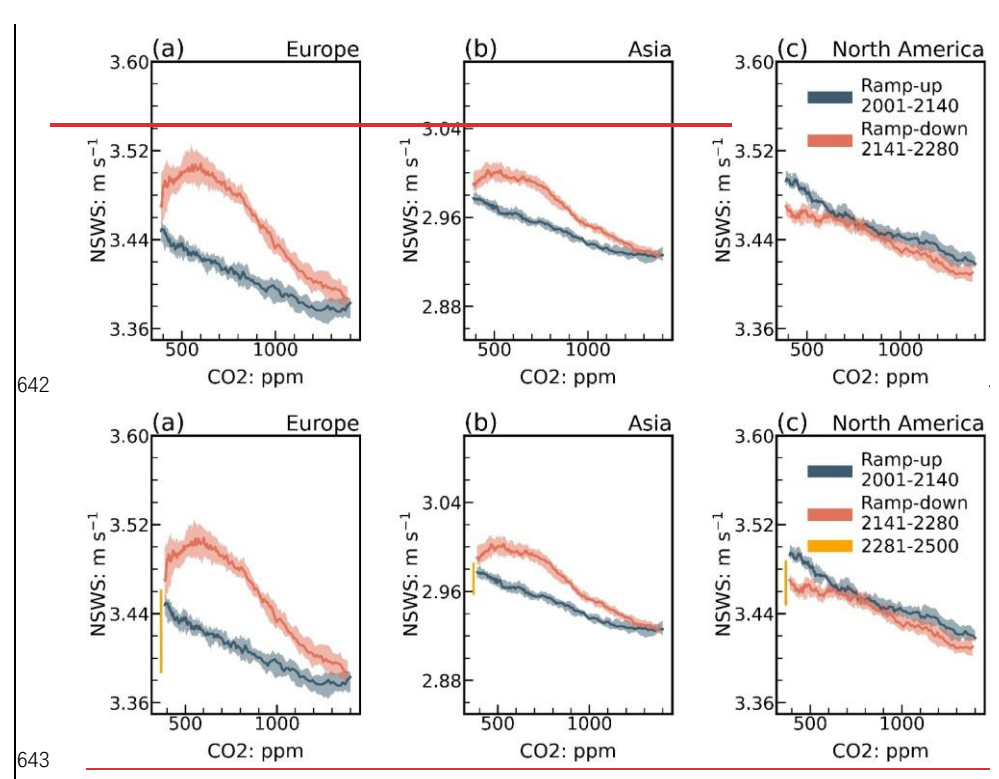


Figure 4. (a) Inter-ensemble correlation coefficients between the 28 ensemble members: the AMOC versus North Atlantic (NA, 60°W–30°E) surface air temperature (SAT) gradient (60°N–90°N minus 0°N–30°N) from 2000 to 2300. Three dashed gray lines denote 2140, 2220 and 2280, respectively. Two dashed blue lines denote the 0.05 significance level. (b) Same as (a), but for correlation coefficients between the AMOC and NA westerly jet strength (30°N–60°N, 60°W–30°E) at 500 hPa. (c) Same as (a), but for correlation coefficients between the AMOC and terrestrial near-surface wind speed (NSWS) over Europe (30°N–60°N, 5°W–60°E). An 11-year running mean has been applied to smooth out inter-annual variability.



**Figure 65.** The physical mechanisms by which CO<sub>2</sub> and Atlantic Meridional Overturning Circulation modulate extratropical near-surface wind speed during three periods.

Formatted: Subscript



**Figure 76.** (a) Changes of terrestrial annual-mean near-surface wind speed over Europe (30°N–70°N, 5°W–50°E) as a function of CO<sub>2</sub> concentrations after 11-year running mean. The ramp-up (dark blue) and), ramp-down (orange), and stabilization (yellow) are denoted with different colors. The solid line represents the ensemble mean, and the shaded area shows the 25th to 75th percentile range of 28 ensemble members. (b-c) Same as (a), but for Asia (20°N–70°N, 60°E–180°E) and North America (30°N–70°N, 170°W–50°W). The range of Y-axis is 0.25 m s<sup>-1</sup> in each subplot.